ELSEVIER

Journal of Photochemistry and Photobiology A: Chemistry 155 (2003) 163–170

Journal of Photochemistry and Photobiology A:Chemistry

www.elsevier.com/locate/jphotochem

Photoelectrochemistry at SnO_2 particulate fractal electrodes sensitized by a ruthenium complex Solid-state solar cell assembling by incorporating a composite polymer electrolyte

T. Stergiopoulos [a], I.M. Arabatzis [a], H. Cachet [b], P. Falaras [a,*]

[a] *Institute of Physical Chemistry, NCSR "Demokritos", 153 10 Aghia Paraskevi, Attikis, Athens, Greece*

[b] *UPR 15 du CNRS "Physique des Liquides et Électrochimie", Université Pierre et Marie Curie, 75252 Paris Cedex 05, France*

Received 11 October 2002; received in revised form 17 October 2002; accepted 28 October 2002

Abstract

Nanocrystalline tin oxide thin film electrodes were prepared and their structural and morphological properties were characterized. X-ray diffraction (XRD) confirmed the films crystallinity, whereas both scanning electron microscopy (SEM) and atomic force microscopy (AFM) revealed the presence of a porous and fractal network of interconnected nanoparticles forming uniform surface features of relatively low roughness. The SnO_2 particulate fractal electrodes were successfully sensitized by the ruthenium N3 complex and solid-state solar cells were assembled by incorporating a binary polymer/inorganic oxide electrolyte. The incorporation of the composite electrolyte consisting of poly(ethylene) oxide (PEO) filled with titanium oxide and containing LiI and I_2 as the redox couple presents a satisfying cell performance in comparison with a liquid junction photoelectrochemical cell: typical maximum incident photon to current efficiency (IPCE) as high as 46% at 510 nm, short-circuit photocurrent (J_{sc}) of 2.6 mA cm^{-2} and overall conversion efficiency (η) of 0.14% under white light illumination were obtained. The IPCE values of the solid-state dye-sensitised solar cells based on SnO_2 are high enough and can be compared to those obtained with titania nanoporous electrodes. The relatively low light to power energy conversion efficiency is attributed to the poor fill factor (FF = 0.21) and photovoltage (V_{oc} = 0.21 V), characteristics that are related to the reduction of triodide by conduction band electrons and the intrinsic properties of tin oxide.

Keywords: SnO_2 particulate films; AFM; Solid-state electrolyte; Dye-sensitized solar cell

1. Introduction

Dye-sensitized solar cells have attracted great scientific and technological interest as potential alternatives to classical photovoltaic devices for their low production cost [1]. Significant advancement made by Nazeeruddin et al. with rough, high surface area titanium dioxide nanocrystalline thin film electrodes sensitized by ruthenium bipyridyl complexes, led to conversion efficiencies up to 10% [2].

Most of the dye-sensitized solar cells are made from nanoporous TiO_2 photoelectrodes; however, the search for new electrode materials is intensive. SnO_2 is a stable, wide band-gap semiconductor (E_g = 3.6 eV) that has been widely used in many electrooptical devices. Compared to TiO_2, SnO_2 is a better electron acceptor since its conduction band edge (E_{cb} = 0.0 V versus NHE) lies ~0.5 V more positive than that of TiO_2 [3].

The tin oxide sensitization mechanism, schematically presented in Fig. 1, is similar to that of titanium dioxide and involves light absorption by the dye resulting in rapid electron injection into the conduction band of the semiconductor. To complete the circuit, the photoexcited adsorbed dye is regenerated from its oxidized state by electron transfer from iodide ions present in the electrolyte phase, which are then reduced at the counter electrode [4].

Although numerous studies of dye injection into colloidal SnO_2 have been published [5–8], no significant works concerning dye-sensitized solar cells based on SnO_2 nanoporous photoanodes were presented so far. Photoelectrochemical cells constructed by Bandara et al. using SnO_2 sensitized with Eosin Y showed V_{oc} of 175 mV and J_{sc} of 50 μA cm^{-2} [9]. Fungo et al. have reported a 8%

* Corresponding author. Tel.: +30-210-650-3644; fax: +30-210-651-1766.
E-mail address: papi@chem.demokritos.gr (P. Falaras).

1010-6030/02/$ – see front matter © 2002 Elsevier Science B.V. All rights reserved.
PII: S1010-6030(02)00394-5

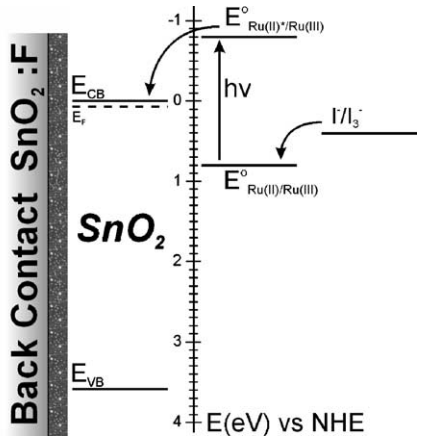

Fig. 1. Energy level diagram for a dye-sensitized nanocrystalline SnO_2 solar cell involving charge injection from the dye excited state-Ru(II)* into the SnO_2 conduction band—CB and dye regeneration via reduction of the oxidized dye-Ru(III) by I^- ions.

incident photon to current efficiency (IPCE) by sensitizing mesoporous tin oxide with porphyrin dyads [10]. Nasr et al. reported a 50% photon to current efficiency at 470 nm with Ru(2,2′-bipyridine)$_2$-(2,2′-bipyridine-4,4′-dicarboxylic acid)$^{2+}$ [11]. A solar light to electrical power conversion efficiency of 0.64% from a mercurochrome-sensitized SnO_2 solar cell was obtained under one sun by Hara et al. [12]. Srivastava et al. prepared nanosized mesoporous tin oxide by a sonochemical approach and obtained a 0.67% conversion efficiency [13]. Ferrere et al. have studied dye sensitization of nanocrystalline SnO_2 electrodes using perylene derivatives with an overall efficiency of 0.89% [14]. Tian et al. presented a 68% IPCE value obtained by a dye-sensitized SnO_2 photoelectrochemical cell utilizing soluble perylene derivatives and cyanine dyes in combination with $RuL_2(SCN)_2$ [15]. Chappel and Zaban have synthesized 18 nm SnO_2 colloids resulting in about 4 mA cm^{-2} and 280 mV as J_{sc} and V_{oc} values, respectively [16]. Kay and Grätzel presented an energy conversion efficiency of 1.2%, by using thicker than 1 μm SnO_2 nanoporous electrodes [17]. Finally, Tennakone et al. reported a 1.3% energy conversion efficiency when the film was 100% SnO_2 [18].

We report here on the spectrophotoelectrochemical properties of the SnO_2 particulate films. We present our results that describe for the first time, to the best of our knowledge, an all solid-state solar cell based on tin oxide nanoelectrodes by using a solvent free composite electrolyte, previously developed in our laboratory [19,20], consisting of high-molecular mass poly(ethylene) oxide (PEO) with the addition of a "solid plasticizer" (commercial TiO_2) in the presence of the I^-/I_3^- redox couple. The addition of inorganic oxides as fillers generally improves the transport properties, the resistance to crystallization and the electrode–electrolyte stability [21]. In parallel, the conductivity (ionic mobility of the iodide/triodide anions) is enhanced due to the enlargement of the amorphous phase in the polymer matrix [22]. The obtained efficiencies of the corresponding dye-sensitized cells are encouraging for this type of systems (n-type semiconductors with large band-gap as SnO_2, ZnO, Nb_2O_5, In_2O_3: polymer solid electrolyte).

2. Experimental

2.1. Preparation of SnO_2 films

Transparent, thin nanostructured SnO_2 films were prepared by a method that follows the procedure described in [23] on F-doped SnO_2 conductive glass substrates (prepared by spray pyrolysis, reported in [24]), ultrasonically cleaned in ethanol prior to use. As starting material, SnO_2 solution was purchased from Nyacol Products as 15 wt.% colloidal dispersion in water with K^+ as counterion (the particle diameter of these colloids is in the range of 10–15 nm) and used without dilution. To facilitate film formation from the sol, one drop of surfactant solution (Triton X-100, Aldrich) was added for each milliliter of the solution. The solution/surfactant mixture was then smeared onto the SnO_2:F substrate by a glass rod. An adhesive tape strip on the conductive glass determines the film thickness. The layer was dried in air at room temperature for 15 min, followed by treatment at a temperature of 450 °C for 30 min in order to ensure an electrical contact between the colloids as well as between the colloids and the substrate.

2.2. Surface modification of SnO_2 films with sensitizer molecules

The dye, Ru(dcbpy)$_2$(NCS)$_2$ [*cis*-bis(isothiocyanato)bis(2,2′-bipyridine-4,4′-dicarboxylic acid)-ruthenium(II)], so-called Ru535 and formerly N3, was purchased from Solaronix SA. Surface derivatization of the tin oxide was achieved by immersing the SnO_2 thin film electrodes overnight in a 10^{-4} dry ethanol solution of the complex. The films were heat-treated for 30 min at 120 °C before immersion, in order to eliminate physisorbed water. Noteworthy that a red color was developed imminently after immersion, implying that a chemical reaction took place and confirming the dye grafting on the semiconductor surface. After completion of the dye adsorption the modified materials were thoroughly washed with ethanol and dried under Ar. Thus, any dye in excess was eliminated and a monolayer coverage of the tin oxide surface was assured.

2.3. Preparation of the composite polymer electrolyte

For the composite electrolyte preparation, 0.0383 g of the filler TiO_2 Degussa P25 (9% w/w), dried for about 24 h at 250 °C, were first dispersed in acetonitrile (CH_3CN). To this dispersion, the I^-/I_3^- redox couple (0.1 g LiI and 0.019 g I_2) was incorporated. Then, the PEO (MW = 2,000,000) was added under continuous stirring. To improve homogeneity and avoid phase discontinuities, the mixture was

sonicated and then stirred for another 24 h. The final product was heated at 70 °C in order to evaporate the solvent.

2.4. Solar cell assembly

The counter-electrode is a F-doped SnO_2 transparent conductive glass on which a very thin platinum layer is sputtered to give a catalytic effect on the electron donor reduction. The electrolyte was sandwiched between the photoelectrode and the platinized SnO_2 counter electrode by firm press. An adhesive tape (approximately 50 μm from 3 M Scotch) was placed between the photoelectrode and the counter electrode to avoid short-circuiting.

2.5. Characterization–surface analysis–absorption characteristics

The SnO_2 film was analyzed with an X-ray diffractometer (Siemens D-500, Cu Kα radiation) to assess the crystallinity of the sample. Detailed surface images were obtained and the film's thickness was determined by the cross section of the image by means of a scanning electron microscope with numerical image acquisition (LEICA S440). Surface morphology, roughness and fractality of the films were also examined with a Digital Instruments Nanoscope III atomic force microscope (AFM), operating in the tapping mode (TM). For the fractal analysis the V423r3 algorithm was used [25,26].

UV-Vis absorption spectra of the modified transparent films were obtained with a Hitachi U-4001 spectrophotometer equipped with an integrating sphere in order to avoid light scattering effects.

2.6. Spectroelectrochemical and photoelectrochemical measurements

The IPCE has been measured as a function of the incident photon current density for different wavelengths. The experimental technique consists of illuminating the cell with a 1000 W Xenon arc lamp in combination with a mini-chrom monochromator. About 10% of the exciting light intensity is sinusoidally modulated and the resulting modulated photocurrent is detected by a Solartron 1250 frequency response analyzer. A cut-off filter was used to exclude wavelengths $\lambda < 400$ nm preventing the generation of electron-hole pairs through direct SnO_2 band-gap excitation. A glass sheet was used as a beam splitter to direct a 50% portion of the incident light beam toward a fast calibrated photodiode (UDT instruments). The photocurrent of the DSSC was measured under short-circuit conditions as a voltage through the resistance of a Solartron 1286 potentiostat and the incident flux at the surface of the photodiode was measured also as a voltage through a radiometer and is detected by the analyzer too. With this setup, the incident photon current density and the photocurrent of the solar cell can be measured simultaneously. The ratio of the above quantities gives access to the number of photoemitted electrons per incident photons (external quantum yield). Because of the very slow photocurrent response of the solid-state dye-sensitized solar cells, the incident light was modulated at a frequency of 50 MHz.

The *I–V* measurements were performed using an Autolab potentiostat (Eco Chemie) controlled by a personal computer. The cell was illuminated by a quartz-halogen lamp that supplies 80 mW cm^{-2} operating in the spectral range 400–700 nm.

3. Results and discussion

3.1. Characterization of SnO_2 films

The sharp and high intensity peaks in the X-ray diffraction (XRD) pattern, presented in Fig. 2, show that the films present very good crystallization. All the reflection peak positions can be indexed as the cassiterite-characteristic modification of SnO_2. In the diffraction pattern of the films, lines which were in good agreement with the crystalline SnO_2 cassiterite standard [27] are the following (their *hkl* indices are given in parentheses): 25.776 (1 1 0), 33.276 (1 0 1), 36.786 (2 0 0), 51.096 (2 1 1), 53.766 (2 2 0), 61.506 (3 1 0), 64.356 (3 0 1), 70.926 (2 0 2), 77.766 (3 2 1) and 83.556 (2 2 2).

Scanning electron microscopy (SEM) was employed to perform at first the surface characterization of the manufactured films. The SEM images, presented in Fig. 3, show that the film exhibits an almost flat and well-distributed network of surface features having certain homogeneity in size and forming pores of about 50 nm. It is clear that the cross section profile (Fig. 3b) gives a thickness of 1.2 μm, uniform all over the films' extension.

To further investigate the morphological characteristics of the SnO_2 films, AFM has been applied, operating in the TM. Fig. 4 presents 2 μm × 2 μm surface plot (three-dimensional

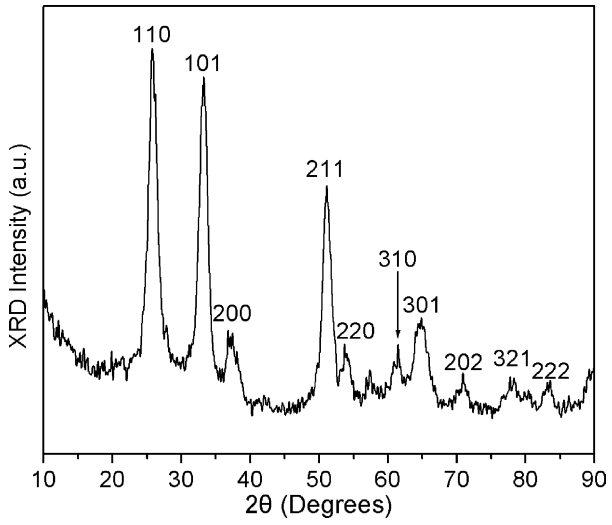

Fig. 2. XRD patterns of nanocrystalline SnO_2 films: cassiterite reflections.

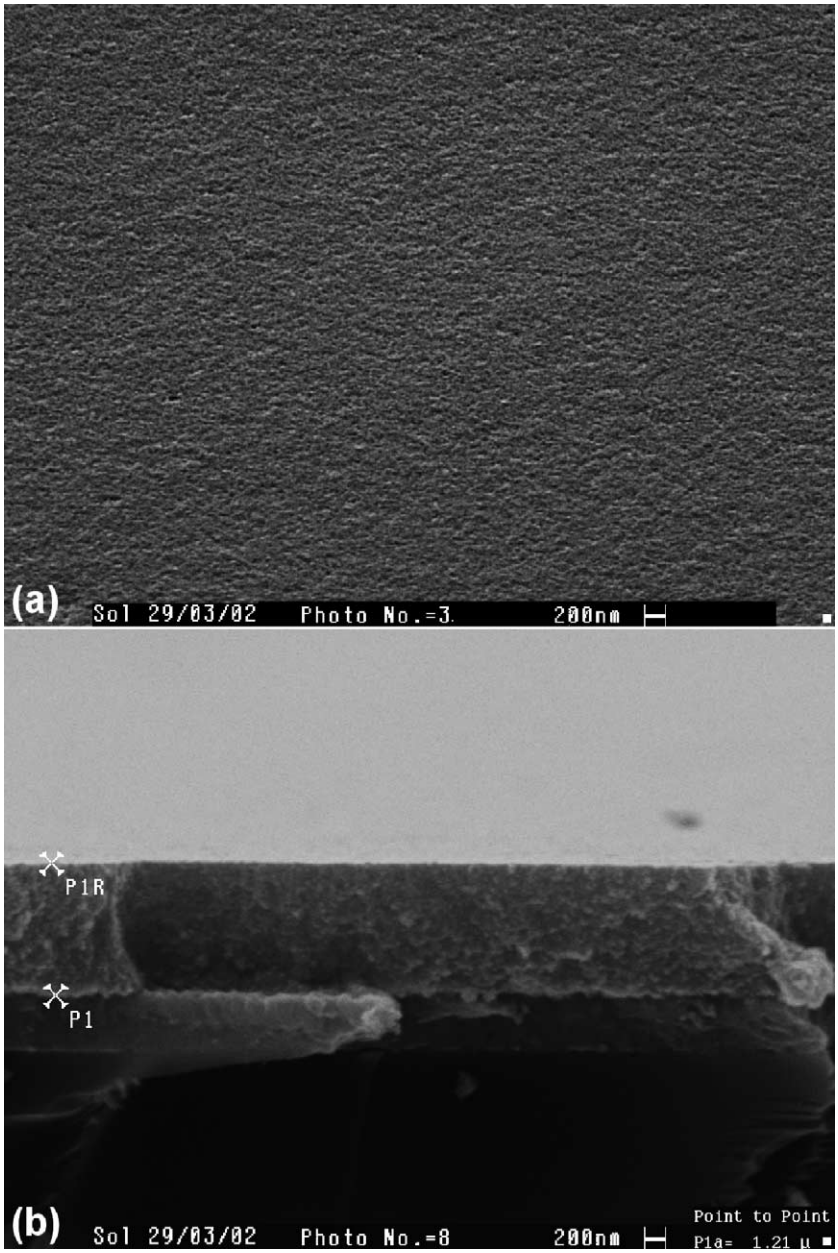

Fig. 3. SEM images of a SnO_2 film: top view (a) and cross section (b).

representation, Fig. 4b) together with top view of the films (Fig. 4a). The films consist of interconnected grain particles, fused together to build up high mountains and deep valleys. Surface parameters such as minimum (average) grain diameter, roughness and fractal dimension are given in Table 1. The average grain diameter is about 22 nm compares well with the particle size of the initial colloid solution. This small difference shows that no significant aggregation occurred during the sintering of nanocrystalline film from SnO_2 colloids. The magnitude of the surface characteristics is considered low (the height histogram shows particles with a Gaussian-like distribution maximum only just 15 nm), when compared to similarly manufactured TiO_2 films [28]. The RMS (standard deviation of the Z values, Z being the total height range analyzed) value of 4 nm listed in Table 1 indicates that the SnO_2 films present characteristics of a flat film surface.

Table 1
Surface parameters of the nanocrystalline SnO_2 films evaluated from the AFM analysis

Average grain diameter (nm)	22
Fractal dimension (D_f)	2.32
Roughness RMS (nm)	4.005
Maximum of height distribution (nm)	15.215

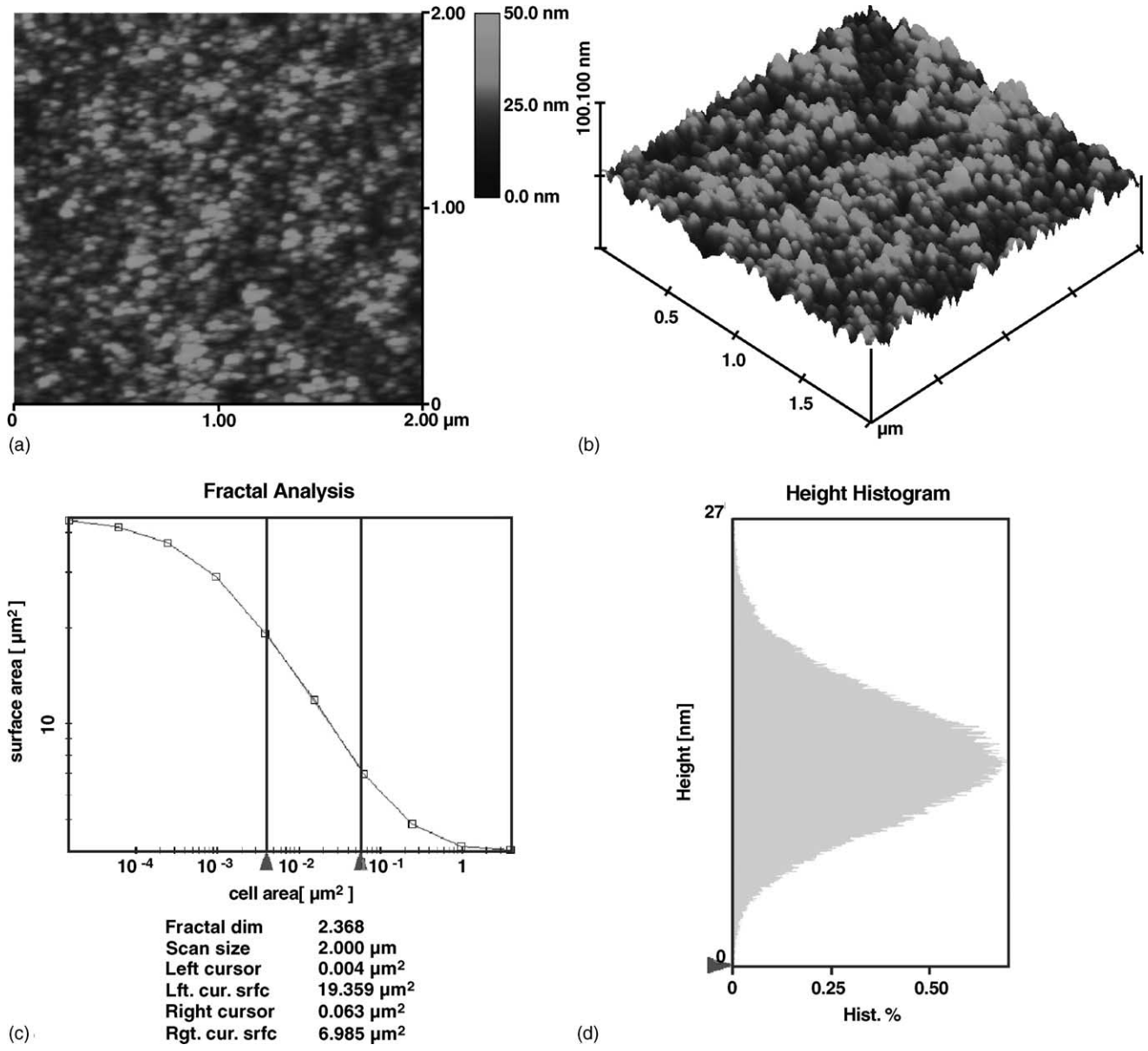

Fig. 4. Top view (a) and three-dimensional surface plot (b) AFM pictures of the nanocrystalline SnO_2 film. Fractal analysis (c) and grain size analysis-height histogram (d).

The SnO_2 films also show a complex topography characterized by a great number of surface features of high frequency. In order to evaluate the geometric complexity of the film surface, qualitative analysis of the fractal dimension parameter (a parameter which reflects the scaling behavior and is an intrinsic property of the material), D_f ($3 \geq D_f \geq 2$) was performed [25,26]. The measured value of fractal dimension was 2.32 (± 0.02) and the fractal analysis has shown that the films exhibit a self-affined scaling character over a significant range of length scales as a consequence of a "chaotic" dynamic deposition process. It is worthwhile mentioning that the fractal dimension characterizes mainly the complexity of the surface and not its texture and roughness.

The fractal dimension (D_f) parameter influences the effective surface extension of the film. In fact, it is well established that the real surface area of the fractal films is several hundred times greater than the one of a flat "Euclidean" non-fractal surface. One can consider that small nanocrystallites of the fractal film act "sponge"-like to capture all the incident photon energy. The fractal SnO_2 films are endowed with a high real surface extension, which could be very benefit for the photosensitization process, as a large amount of surface sites is available for the binding of the dye molecules. Such a complicated surface creates an irregular environment where multiple light reflection can occur, thus considerably increasing the amount of the adsorbed photons. Furthermore, the porous photoelectrode surface permits a better "wetting"

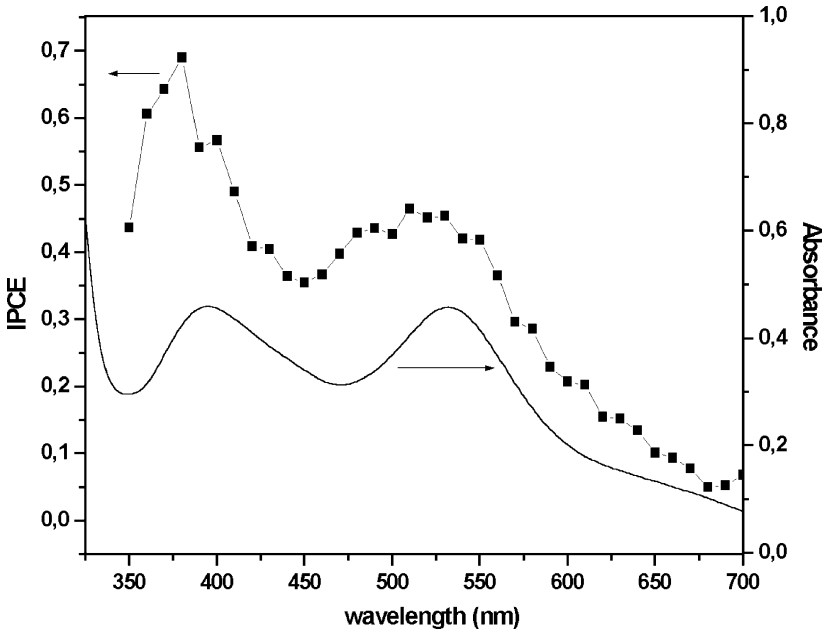

Fig. 5. Photocurrent action (IPCE) spectrum of the SnO_2/Ru535 system with illumination through the conductive substrate and absorption spectrum of SnO_2 obtained after modification with the dye.

of the film by the composite electrolyte and finally results in a perfect penetration of the I^-/I_3^- redox couple into the film pores, which in turn favors the interaction between the oxidized dye and regeneration of the sensitizer's ground state.

3.2. Absorption and photoelectrochemical properties of sensitized SnO_2 electrodes

The absorption spectrum of Ru535 adsorbed on SnO_2 is shown in Fig. 5. Modified electrodes exhibit strong absorption in the visible confirming the binding of the sensitizer to the semiconductor surface. The coloration of the SnO_2 film was much weaker than that of a TiO_2 electrode of similar geometric surface size. This is explained by the more acidic character of the SnO_2 surface, whose isoelectric point is at pH 4–5 as compared to pH 6.2 for TiO_2 anatase [29], but also by differences in thickness, roughness and surface characteristics.

All solid-state dye-sensitized solar cells of the type

$$SnO_2 : F/SnO_2\text{-dye}//\text{electrolyte}//Pt/SnO_2 : F$$

were fabricated using the PEO/TiO_2/I^-/I_3^- composite electrolyte. The photoelectrochemical properties of these cells were investigated under short-circuit conditions. This solar cell can efficiently convert visible light in the region from 400 to 700 nm to photocurrent, as shown in Fig. 5. The close match between the photocurrent action spectrum and the absorption spectrum indicates that photosensitization mechanism is operative in generation of photocurrent. The generation of anodic current is indicative of the fact that the direction of flow of electrons is toward the conductive substrate. IPCE represents the percentage of incident photons that are converted to electrons at a certain wavelength and is defined by the formula

$$\text{IPCE}(\lambda) = 1240\left(\frac{I_{sc}}{\lambda\Phi}\right) \quad (1)$$

where λ is the wavelength (in nanometers) and Φ is the incident radiative flux (in units of $W\,m^{-2}$) [30]. Typical maximum IPCE as high as 46% were obtained at 510 nm, a value which is comparable with that obtained with liquid electrolytes [31]. Very efficient IPCEs indicate that electron transfer process from excited dye to the conduction band of SnO_2 occurs effectively due to the fact that the necessary driving force for the rapid vectorial charge displacement is efficiently high, about 0.5 eV [32]. In addition, electron transfer from I^- ion to oxidized dye is also an effective process, feature that indicates good "wetting" of the semiconductor film by the solid composite polymer electrolyte, which gives rise to a penetration into the nanoporous structure of the film. In order to rationalize the above observations, the monochromatic current yield is expressed in terms of light harvesting efficiency (LHE), the quantum yield of charge injection (ϕ_{inj}) and the efficiency of collecting the injected charge at the back contact (n_c) [2]:

$$\text{IPCE}(\lambda) = \text{LHE}(\lambda)\phi_{inj}n_c \quad (2)$$

By taking into account the fact that the SnO_2/Ru(II) film absorbs the 46% of the incident photons and that the same percentage of these photons is converted to electrons through the external circuit, including the fact that $\phi_{inj} > 99.9\%$ for the Ru(II) complex $RuL_2(H_2O)$ [33], one can claim that

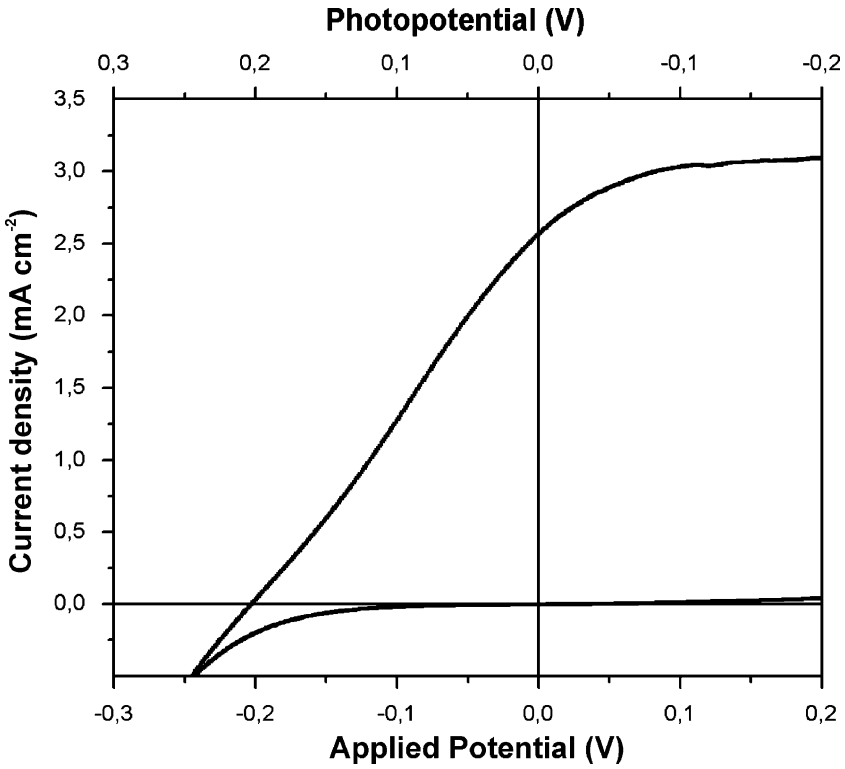

Fig. 6. Current–voltage characteristics in the dark (lower curve) and under illumination of the SnO_2/Ru535 dye-sensitized solar cell using the PEO/TiO_2 composite polymer electrolyte. Area: 0.225 cm^2; white light illumination by a quartz-halogen lamp: 80 mW cm^{-2}; V_{oc} = 0.21 V; J_{sc} = 2.6 mA cm^{-2}; FF = 21%; η = 0.14%.

the efficiency of collecting the injected charge at the back contact is practically 100%.

Fig. 6 exhibits the current–voltage characteristics of such a typical dye-sensitized solar cell employing the PEO/TiO_2/redox couple composite polymer electrolyte, measured with a white light lamp providing 80 mW cm^{-2} in the spectral region 400–700 nm. The solar energy conversion efficiency (η) reached only 0.14%, with a large short-circuit current density (J_{sc}) of 2.6 mA cm^{-2}, an open-circuit photovoltage V_{oc} of 0.21 V and a very poor fill factor (FF = 0.21). Upon illumination, the photogenerated electrons in the dye are transferred to the conduction band of the semiconductor. Consequently, the Fermi level or electrochemical potential of the nanocrystalline SnO_2 film of the semiconductor moves very close to the conduction band, and the maximum photovoltage that one can obtain is the energy difference between the pseudo-Fermi level of the semiconductor under illumination and the oxidation potential of the redox couple present in the electrolyte [11]. For regenerative photoelectrochemical system, the following equation holds [34]:

$$V_{oc} = \left(\frac{kT}{e}\right) \ln\left(\frac{I_{inj}}{n_{cb} k_{et}[I_3^-]}\right) \quad (3)$$

where I_{inj} is the flux of charge resulted from dye-sensitized electron injection, n_{cb} the concentration of electrons within the conduction band of SnO_2, and k_{et} is the rate constant for triiodide reduction. Taking into consideration the E_{ox} of the I^-/I_3^- couple ~0.5 V versus NHE [35] and the reported values of E_{cb} for SnO_2 (0.0 V versus NHE, corresponding to the electron affinity of SnO_2 = 4.5 eV with respect to the vacuum level), the cell should furnish maximum photovoltage 500 mV. The actual band edge position may be somewhat different when in contact with the solid redox electrolyte. The obtained value, however, is much smaller than the theoretical predicted values due to the recombination process and obviously lower than that obtained with TiO_2 (typically $V_{oc} \approx$ 700 mV [19,20]). Such reduced values of fill factor and photovoltage (accordingly to the above equation) are attributed to charge recombination reaction at the nanocrystalline/redox electrolyte interface [36]:

$$2e^- + I_3^- \rightarrow 3I^- \quad (4)$$

The above reduction of triiodide by conduction band electrons can be identified by the rapid rise of a cathodic dark current during the cell operation (onset of dark current at about −110 mV as shown in Fig. 6). However, the main cause for poor efficiency is the high internal series resistance of the order of 100 Ω cm^{-2}, obtained from the slope of the quasi-linear current–voltage curve in Fig. 6 and confirmed by impedance measurements. The ohmic drop at 2 mA cm^{-2} would reach about 200 mV, shifting the photocurrent plateau (in principal proportional to the light flux) toward positive potentials.

The main reason for efficiency losses should be connected to the small particle diameter and the limited thickness of the SnO_2 films. The above features are major limiting factors, because faster electron migration may result from improved electrical conductivity that is expected when larger nanoparticles are sintered together [37] and on the other hand, the amount of photogenerated charge carriers increases with increasing thickness [3]. Especially, the thickness of a layer made from the solution limited to 1 μm, is a factor that we tried to control by simple deposition of different layers. However, electrodes that could be thicker by successive deposition—when sintering follows each deposition—suffered from lateral inhomogeinity. Moreover, in this fabrication process, a perpendicular to the substrate inhomogeinity relating to the size of the pores and the electrical conductivity was induced, when each colloid has experienced a different sintering duration depending on its distance from the substrate [16].

4. Conclusions

In summary, we have presented an all solid-state dye-sensitized solar cell based on SnO_2 electrodes by using a composite solid electrolyte. Surface properties of tin oxide films were investigated showing an almost flat and complicated surface defined by a three-dimensional network consisted of small crystallites of cassiterite in close contact with each other, with high efficiency in light capture and dye loading. Photoelectrochemical measurements indicate that the cells present high short-circuit photocurrents, in contrast with related low overall energy conversion efficiencies.

As for the role of the composite polymer electrolyte, our results up to now present outstanding overall conversion efficiency (about 4%) of the corresponding solid-state dye-sensitized TiO_2 solar cell and thus excellent “wetting” of the semiconductor film by the solid electrolyte is believed to take place [20]. However, as the nature of the filler plays a significant role to the performance of such an electrolyte [38], we can apply the same material for both the semiconductor film and the filler (SnO_2 powder). This will probably allow a more uniform particle distribution at the dye-coated semiconductor/electrolyte interface and further improvement of the photovoltaic performance of the corresponding solar cells is expected. Yet, the incorporation of a new redox couple Br^-/Br_2 instead of I^-/I_3^- will produce a positive difference in the photovoltage caused by the difference between the solution potentials of the redox couples, which were measured to be +0.535 and +0.115 V versus SCE, respectively [14].

Acknowledgements

Thanks must be addressed to SPCI S.A. Saint Denis-France and Nyacol Nano Technologies Inc. for generously providing the SnO_2 colloidal solution. This work has been supported by France–Greece (Platon) bilateral cooperation project. T. Stergiopoulos thanks the French Government (CIES) for fellowship allowance. Finally, the authors would like to express gratitude to Stephan Borensztajn for taking the SEM images.

References

[1] B. O’Regan, M. Grätzel, Nature 353 (1991) 737.
[2] M.K. Nazeeruddin, A. Kay, I. Rodicio, R. Humphry-Baker, E. Müller, P. Liska, N. Vlachopoulos, M. Grätzel, J. Am. Chem. Soc. 115 (1993) 6382.
[3] I. Bedja, S. Hotchandani, P. Kamat, J. Phys. Chem. 98 (1994) 4133.
[4] A. Hagfeldt, M. Grätzel, Chem. Rev. 95 (1995) 49.
[5] D. Noukakis, M. van der Auwaraer, F.C. De Schryver, J. Phys. Chem. 98 (1994) 11745.
[6] W. Ford, M.A.J. Rodjers, J. Phys. Chem. 99 (1995) 5139.
[7] D. Liu, P. Kamat, J. Electrochem. Soc. 142 (1995) 835.
[8] L. Tan-Sien-Hee, A.K. de Mersmaeker, J. Electroanal. Chem. 406 (1996) 147.
[9] J. Bandara, K. Tennakone, P.P.B. Jayatilaka, Chemosphere 49 (2002) 439.
[10] F. Fungo, L.A. Otero, L. Sereno, J.J. Silber, E.N. Durantidi, J. Mater. Chem. 10 (2000) 645.
[11] C. Nasr, P. Kamat, S. Hotchandani, J. Phys. Chem. B 102 (1998) 10047.
[12] K. Hara, T. Horiguchi, T. Kinoshita, K. Sayama, H. Sugihara, H. Arakawa, Sol. Energy Mater. Sol. C 64 (2000) 115.
[13] D.N. Srivastava, S. Chappel, O. Palchik, A. Zaban, A. Gedanken, Langmuir 18 (2002) 4160.
[14] S. Ferrere, A. Zaban, B.A. Gregg, J. Phys. Chem. B 101 (1997) 4490.
[15] H. Tian, P.-H. Liu, F.-S. Meng, E. Gao, S. Cai, Synth. Metals 121 (2001) 1557.
[16] S. Chappel, A. Zaban, Sol. Energy Mater. Sol. C 71 (2002) 141.
[17] A. Kay, M. Grätzel, Chem. Mater. 14 (2002) 2930.
[18] K. Tennakone, P.K.M. Bandaranayake, P.V.V. Jayaweera, A. Konno, G.R.R.A. Kumara, Physica E 14 (2002) 190.
[19] G. Katsaros, T. Stergiopoulos, I.M. Arabatzis, K.G. Papadokostaki, P. Falaras, J. Photochem. Photobiol. A: Chem. 149 (2002) 191.
[20] T. Stergiopoulos, I.M. Arabatzis, G. Katsaros, P. Falaras, Nanoletters 2 (2002) 1259.
[21] J.E. Weston, B.C.H. Steele, Solid State Ionics 7 (1982) 75.
[22] C. Capiglia, P. Mustarelli, E. Quarterone, C. Tomasi, A. Magistris, Solid State Ionics 118 (1999) 73.
[23] B.I. Lemon, J.T. Hupp, J. Phys. Chem. B 101 (1997) 2426.
[24] J. Bruneaux, H. Cachet, M. Froment, A. Messad, Electrochim. Acta 39 (1994) 1251.
[25] A. Provata, P. Falaras, A. Xagas, Chem. Phys. Lett. 297 (1998) 484.
[26] P. Falaras, A.P. Xagas, J. Mater. Sci. 37 (2002) 3855.
[27] JCPDS Powder Diffraction File, Card 21-1272, JCPDS, International Centre for Diffraction Data, Swarthmore, PA, 1980.
[28] P. Falaras, Sol. Energy Mater. Sol. C 53 (1998) 163.
[29] G.A. Parks, Chem. Rev. 65 (1965) 177.
[30] C.J. Barbé, F. Arendse, P. Comte, M. Jirousek, F. Lenzmann, V. Shklover, M. Grätzel, J. Am. Chem. Soc. 80 (1997) 3157.
[31] P. Kamat, I. Bedja, S. Hotchadani, L.K. Patterson, J. Phys. Chem. 100 (1996) 4900.
[32] H. Gerischer, Top. Appl. Phys. (1979) 115.
[33] R. Eichberger, F. Willig, Chem. Phys. 141 (1990) 159.
[34] M.L. Rosenblut, N.S. Lewis, J. Phys. Chem. 93 (1989) 3735.
[35] A.J. Bard, R. Parsons, J. Jordan, Standard Potentials in Aqueous Solution, Marcel Dekker, New York, 1985.
[36] S.Y. Huang, G. Schlichthörl, A.J. Nozik, M. Grätzel, A.J. Frank, J. Phys. Chem. B 101 (1997) 2576.
[37] S.T. Aruna, S. Tirosh, A. Zaban, J. Mater. Chem. 10 (2000) 2389.
[38] W. Wieczorek, Z. Florjanczyk, J.R. Stevens, Electrochim. Acta 40 (1995) 2251.